β-graphene monoxide: Two-dimensional crystal form of carbon monoxide

Danylo Radevych,[1,2] Marija Gajdardziska-Josifovska,[1,2,*] Carol J. Hirschmugl,[1,2]
Marvin A. Schofield,[1,2] and Michael Weinert[1]

[1]*University of Wisconsin-Milwaukee, Department of Physics, 3135 N Maryland Ave, Milwaukee, Wisconsin 53211, USA*
[2]*COnovate Inc., 1408 E Olive St, Milwaukee, Wisconsin 53211, USA*

(Received 28 March 2022; accepted 7 July 2022; published 26 July 2022)

A high-symmetry D_{6h} form of graphene monoxide, labeled β-GmO, is proposed based on selected area electron diffraction (SAED) and high-resolution transmission electron microscopy (HRTEM) experiments and density functional theory (DFT) modeling. Joining the previously observed lower symmetry D_{2h} form of two-dimensional (2D) solid CO, now relabeled as α-GmO, this work demonstrates that multiple solid phases are possible in 2D- and 3D-CO. A unit of the β-GmO primitive cell – 1,4,7-trioxacyclononane – is composed of three 1,3-dioxetane units of the α-GmO primitive cell. The invariance of the SAED spots as the sample is tilted prove that β-GmO is composed of large area monolayers, randomly translated with respect to each other, as they form a multilayer stack. In contrast, α-GmO domains rotate with respect to each other and have smaller in-plane domain areas for similar synthesis conditions. *Ab initio* computations demonstrate that β-GmO monolayers generally do not have preferred stacking order and thus do not form three-dimensional (3D) crystal structure. The β-GmO monolayer is predicted to be a 1.2 eV direct band-gap semiconductor and generally softer than both graphene and α-GmO.

DOI: 10.1103/PhysRevMaterials.6.074006

I. INTRODUCTION

Graphene monoxide (GmO) is a novel two-dimensional crystalline material that is the first known solid form of carbon monoxide (CO) found to exist at ambient conditions, both experimentally [1] and via *ab initio* modeling [1–4]. Solid molecular CO is well known in the astrophysics literature; recent review articles list carbon monoxide as the second most abundant molecule on icy grains in the interstellar medium and found on cold planets, moons, and comets [5,6]. Here, we briefly review known laboratory-based crystallographic phases of 3D-CO and report the discovery of the second 2D-GmO crystallographic phase, named β-GmO.

Solid 3D forms of molecular CO were studied in the past and their phase diagram was solidified in the 1980s. The first works reported experimental proof of the α ($P2_13$), β ($P6_3/mmc$), δ (Pm3n), and ε (R3c) solid phases along with P vs. T phase diagram [7–9]. It was concluded that CO undergoes a liquid to solid transition to form β-CO after cooling to 68.2 K at ambient pressure, and then transforms into α-CO after further cooling to 61.5 K. During compression at room temperature ($\sim$297 K), CO goes from liquid to solid β-CO at about 2.5 GPa, then δ-CO is formed at about 4.8 GPa. ε-CO results from liquid or α-CO compressed at low temperature ($\sim$15 K) to about 3.4 GPa. These CO crystal structures are examples of molecular crystals, and more recent reexaminations investigated whether some are polymeric in nature.

Theoretical modeling at pressures greater than 2 GPa and at zero temperature [10] indicated that the molecular Pbcm structure formed with 1,2-dioxetane units became more stable than the α phase at $>$0.5 GPa and 0 K [10]. At zero pressure and temperature, it was noted that polymeric polycarbonyl chains $P2_1/m$ and Pnma, containing double and single bonds, are the most energetically favorable [11,12]. Another lower-energy polymeric structure of $Pna2_1$ symmetry was found with an *ab initio* random structure searching method at 0 GPa and 0 K [12]. The $Pna2_1$ structure was verified by molecular dynamics computations at 300 K to be stable. All these structures, besides the first known α, β, δ, and ε phases, are still purely computational and without experimental proof.

One of the first systematic modeling studies of the two-dimensional layered oxidized graphene at zero temperature and pressure for different C_xO configurations was performed with a genetic algorithm by Xiang *et al.* [13]. The paper reported two lowest-energy structures with C : O ratio of 1, having C_{2v} and D_{2h} symmetry, respectively. Although the C_{2v} structure did not find further development in the literature due to its low symmetry, the D_{2h} structure [Fig. 1(b)] was independently discovered in experiment and DFT simulations by Mattson *et al.* [1] around the same time as Xiang *et al.* The D_{2h} form (space group #65 D_{2h}^{19} Cmmm) was essentially the first known 2D solid form of carbon monoxide found to be stable at room temperature and ambient pressure. It was named graphene monoxide (GmO) to avoid confusion with CO gas and solid graphene oxide (GO) that has lower oxygen content, as well as to underline its two-dimensional character connected to graphene, Fig. 1(a).

Inspired by the multiple phases of 3D-CO crystals, our searches of other monolayer forms of GmO lead to consider-

*mgj@uwm.edu

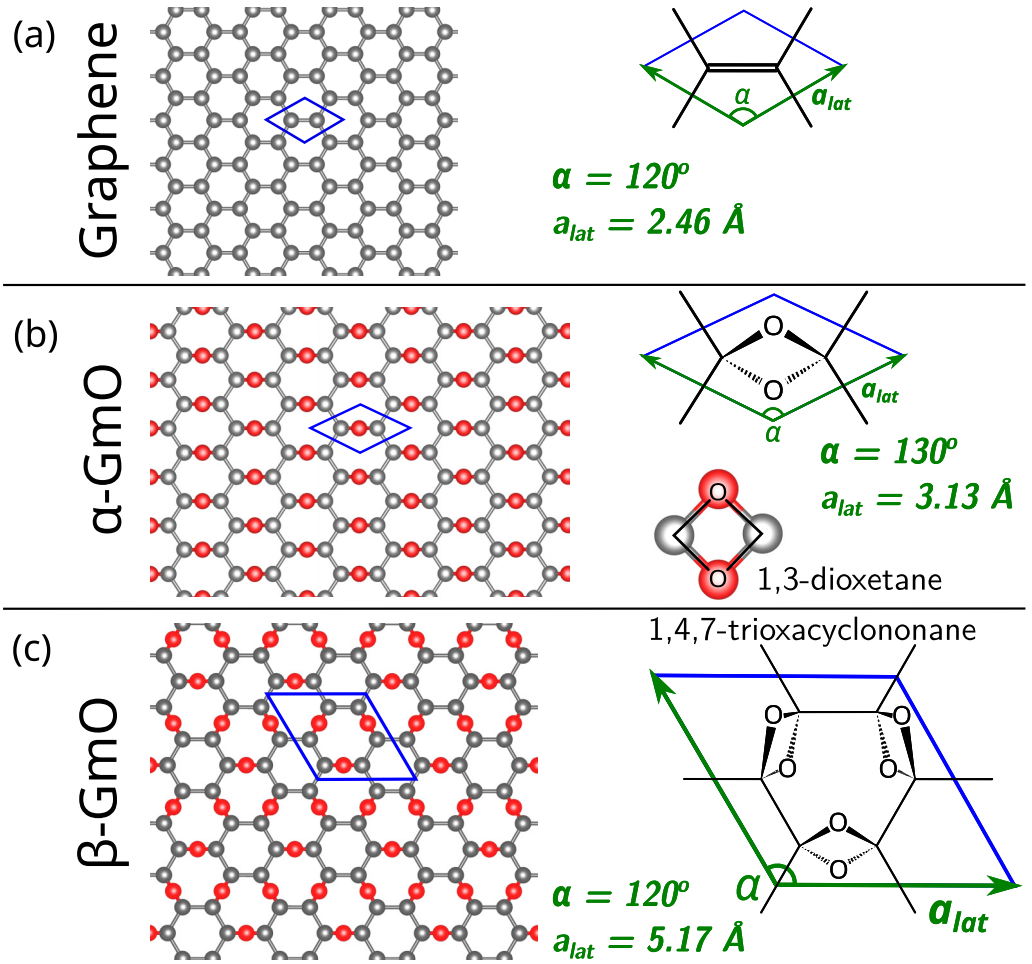

FIG. 1. Atomic structures and bonds with the unit cells of monolayers of (a) graphene, (b) α-GmO, and (c) β-GmO drawn to scale. (Primitive cell borders: blue; primitive lattice vectors: green; C: gray; O: red.)

ation of another higher-symmetry form of oxidized graphene with a C:O ratio of 1 that belongs to the space group #191 D^1_{6h} P6/mmm [Figs. 1(c) and 3], and is predicted to be stable by DFT. This phase was recently discovered by electron diffraction in the transmission electron microscope (TEM)

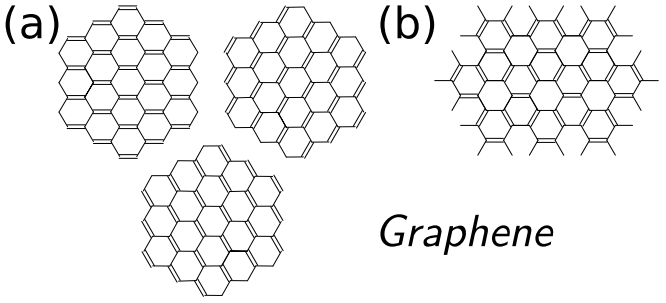

FIG. 2. Double-bond ordering in the infinite periodic monolayer of graphene with sp^2 hybridized C atoms: (a) three equally probable periodic configurations with parallel double bonds aligned in one armchair direction for each configuration, (b) three sets of parallel double bonds aligned along the three armchair directions in one monolayer. Cells in (a) and (b) are drawn to scale.

at ambient temperature and low pressure ($\sim 10^{-4}$ Pa) during measurements on graphene nanocomposite samples created by COnovate Inc., shown later in Figs. 6(a) and 7. To distinguish this higher symmetry monolayer with the same C:O ratio of 1 from the previous one, greek letters in chronological order will be used: the D_{2h} form will be denoted as α-GmO and D_{6h} one as β-GmO.

The double bonds in the infinite periodic monolayer of graphene with sp^2 hybridized C atoms can be represented in two ways: as a resonant state between three equally probable periodic configurations with parallel double bonds aligned in a single armchair direction for each configuration [Fig. 2(a)]or as 3 sets of parallel double bonds aligned along 3 armchair directions within the same monolayer [Fig. 2(b)]. If α- and β-GmO monolayers are formed by breaking double bonds of graphene [Fig. 1(a)], attaching O atoms above and below the carbon plane to form 1,3-dioxetane units [Fig. 1(b) and 1(c)] and making sp^3 C orbitals, then α-GmO corresponds to graphene from Fig. 2(a), where the double bonds align along one of the three equivalent directions differing by a 60° rotation. Similarly, β-GmO corresponds to graphene from Fig. 2(b), where three sets of double bonds are already aligned along the three directions. The evidence, structural, and

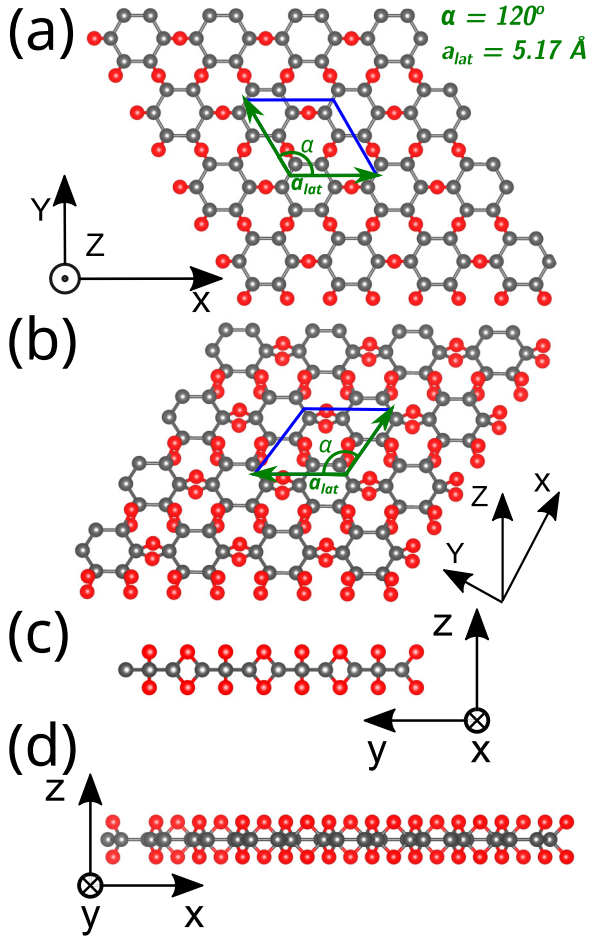

FIG. 3. β-GmO 4×4 supercell in four different views: (a) top, (b) perspective, (c) front, and (d) side. Lattice constant $a_{lat} = 5.17$ Å, opening angle $\alpha = 120°$. O atoms are at ± 1.04 Å from the carbon plane. (Primitive cell borders: blue; primitive lattice vectors: green; C: gray; O: red.)

electronic properties for β-GmO are reported in this work and compared to those of α-GmO.

II. METHODS

A. Density functional theory simulations of structure and electronic properties

Density functional theory (DFT) computations were performed using Quantum ESPRESSO 6.5 [14,15] and structures were visualized via XCrySDen 1.6.2 [16] and VESTA 3.4.8 [17]. Projector augmented-wave (PAW) scalar-relativistic pseudopotentials with the Perdew-Burke-Ernzerhof (PBE) generalized gradient approximation for exchange correlation for C and O atoms were taken from PS library 1.0.0 [18]. A plane wave kinetic energy cutoff of 50 Ry (680 eV) for the expansion of the wave functions and kinetic energy cutoff of 326 Ry (4435 eV) for the charge density and potential were used. The following Monkhorst-Pack k-point meshes were used: $18 \times 18 \times 1$ for graphene and α-GmO primitive cells, and $10 \times 10 \times 1$ for the β-GmO primitive cell; unless otherwise stated, other cells have k-point meshes rescaled accordingly.

B. Electron diffraction modeling

DFT-optimized atomic positions of β-GmO were used to model theoretical electron diffraction patterns, which were compared with experimental selected area electron diffraction (SAED) patterns recorded with 300 keV electrons and illumination conditions that approximate incident plane wave.

Projected two-dimensional unit cells were used for monolayer, bilayer, and trilayer configurations that are translated with respect to each other in a series of stacking combinations. Single-scattering electron diffraction theory was used in light of the relatively weak atomic scattering factors of carbon and oxygen. Non-zero diffraction intensity was obtained only at $\boldsymbol{K}$ rods of the reciprocal space (conservation of momentum). Conservation of energy was modeled by a flat Ewald sphere approximation.

At a given $\boldsymbol{K}$ point of reciprocal space, the diffraction intensity $I_{\boldsymbol{K}}$ is defined as the square modulus of the structure factor $S_{\boldsymbol{K}}$ calculated as the Fourier transform of the atomic scattering form factors $f_j(\boldsymbol{K})$ over the primitive unit cell containing n atoms in jth occupied fractional position $\boldsymbol{d}_j$ in the basis. The atomic form factors for C and O atoms were approximated as a sum of five Gaussians following Peng *et al.* [19]. Theoretical positions and intensities of diffraction peaks for the two-dimensional structures were simulated with this approach with relaxed atomic positions and cell parameters taken from DFT calculations.

C. Synthesis of GmO-containing material

The studied material was synthesized by mixing a carbon-containing source with a source containing transition metal (TM) followed by annealing in high vacuum at variable temperature rates up to 800°C. Commercial graphene oxide (0.4 wt% GO) aqueous suspension was used as a carbon source. Ammonia heptamolybdate [(1.27 g of $(NH_4)_6Mo_7O_{24} \cdot 4H_2O$ per 1 L of H_2O)] was the TM source used. The two liquids were mixed in 1 : 1.5 ratio and mechanically stirred for several minutes at room temperature before poured to dry at 52°C in a dehydrator to produce a film with ~25 μm uniform thickness. The material was annealed at a base pressure of 2×10^{-6} torr to a final temperature of approximately 780 °C over three days (Sample 4.3 from Table 4 in Patent Application [20]). Upon cooling, a small amount of this sample was crushed in a mortar and pestle, suspended in clean methanol, and dropped on a copper TEM grid covered with an ultrathin amorphous carbon film. The dried sample was inserted in the vacuum of the electron microscope for imaging and diffraction studies.

D. Electron diffraction and microscopy experiments

Experimental data were obtained using a Hitachi H-9000NAR high-resolution transmission electron microscope (HR-TEM) operated at 300 kV. Selected area electron diffraction (SAED) patterns were recorded from electron-transparent samples by using an aperture to select contributing sample regions ranging from 500 nm to 2.5 μm in diameter. Amplitude-contrast bright-field TEM images were recorded to obtain the morphology of the diffracting material, and phase-contrast HRTEM images were recorded to obtain the projected atomic lattice of the imaged material. A Gatan

TABLE I. Structure parameters for the graphene, α-GmO, and β-GmO monolayers. Lattice parameter, a_{lat}, bond lengths, and oxygen heights (h_O) are in Å; formation energy, ΔE, in eV/atom; and opening angle, α and bond angles in degrees. 1,3-dioxetane corresponds to an isolated unit.

				Lattice		Bond lengths			Bond angles			
Structure	Space group			a_{lat}	α	C-O	C-C[a]	C-C[b]	C-O-C[c]	C-C-C[d]	h_O	ΔE
Graphene	191	D^1_{6h}	P6/mmm	2.46	120		1.42			120		
α-GmO	65	D^{19}_{2h}	Cmmm	3.13	130	1.44	1.58	1.97	87	114	±1.04	−0.58
α-GmO$^{120^\circ}$	65	D^{19}_{2h}	Cmmm	2.94	120	1.41	1.64	1.83	80	128	±1.08	−0.32
β-GmO	191	D^1_{6h}	P6/mmm	5.17	120	1.43	1.60	1.98	87	120	±1.04	−0.51
1,3-dioxetane						1.40		1.96	88		±1.01	+0.59

[a]Bridge between two connected C atoms without O atoms on top and bottom.
[b]Distance between two non-connected C atoms measured in the 1,3-dioxetane unit.
[c]Measured in the 1,3-dioxetane unit.
[d]In the plane of C atoms.

Orius 4.2 Mpx 14-bit CCD camera was used to convert the high-energy electrons into light and record all imaging and diffraction data digitally. In contrast to the prior creation and observation of nanograms of α-GmO inside the vacuum of the microscope column ($\sim 5 \times 10^{-5}$ Pa) by *in situ* heating [1], the samples in this study were created *ex situ* and were observed at room temperature in the microscope. These samples were scaled up and provided by COnovate Inc., with details described in [20].

III. RESULTS

A. DFT predicted structure

The proposed *ab initio* β-GmO structure computed at zero temperature and pressure is shown in top, perspective, side, and front view in Fig. 3. It was constructed as an isolated monolayer, separated by 25 Å of vacuum in a periodically continued supercell (equivalent to the modeling of α-GmO monolayers), based on different possible double-bond ordering in the infinite monolayer of graphene (Fig. 2). It was assumed that 1,3-dioxetane units [Fig. 1(b)] are formed by breaking C double bonds and attaching O atoms to sp^3 hybridized C atoms, as shown in Fig. 1. Then α-GmO would be produced from graphene in Fig. 2(a), and β-GmO would be built from graphene in Fig. 2(b). In both structures, all C atoms are identical, and every C atom forms four bonds: two with other C atoms and two with O atoms. While 1,3-dioxetane units in α-GmO are aligned in the same "armchair" direction [Fig. 1(b)] (space group #65 D^{19}_{2h} Cmmm), in β-GmO they are aligned in the three equivalent orientations [Fig. 1(c)] such that β-GmO belongs to the higher-symmetry space group #191 D^1_{6h} P6/mmm – the same space group as graphene. The primitive cell of β-GmO has three 1,3-dioxetane units in the 1,4,7-trioxacyclononane ring configuration [Fig. 1(c)] versus only one unit in α-GmO primitive cell [Fig. 1(b)].

The primitive hexagonal cell of a β-GmO monolayer, containing six O and six C atoms, has an opening angle of 120° with a lattice constant of 5.17 Å and O atoms placed ±1.04 Å from the carbon plane. The β-GmO unit cell parameters are approximately in a $(\sqrt{3} \times \sqrt{3})$ R30° relationship with the α-GmO unit cells, and in both the sp^3 C bonds in 1,3-dioxetane are roughly 35% longer than the sp^2 C bonds in graphene. Because of the close structural relationship among the phases, β-GmO, α-GmO, and graphene may form periodic Moiré superlattices; e.g., a $\sqrt{7} \times \sqrt{7}$ β-GmO superlattice and a $\sqrt{31} \times \sqrt{31}$ graphene supercell, both of which are hexagonal, would have a lattice mismatch of less than 0.1%.

The difference of the charge density of the β-GmO relative to free C and O atoms, $\Delta\rho$, is shown in Fig. 4(a) and 4(b), and demonstrates the effect of bonding. Figure 4(c) compares the planar-averaged electron densities, $\Delta\lambda$, of α- and β-GmO. The essentially similar curves demonstrate that the 1,3-dioxetane bonding is the same in both of these 2D CO phases, with the minor differences related to different bond lengths and bond angles between the C and O atoms (see Table I) in the two phases.

Table I compares different structural parameters of the monolayers predicted by DFT. The formation energy of β-GmO is $\Delta E = -0.51$ eV/atom. This value is less negative than $\Delta E = -0.58$ eV/atom of the fully relaxed semiconducting α-GmO configuration (α-GmO); however, it is more negative than the $\Delta E = -0.32$ eV/atom of the constrained conducting α-GmO structure with opening angle $\alpha = 120^\circ$ (α-GmO$^{120^\circ}$, with the same unit cell area as the fully relaxed α-GmO) that is observed to be dominant in the experimental α-GmO–graphene nanocomposite synthesis to date [Fig. 6(b)] [1,20]. DFT-based phonon calculations confirmed that the proposed β-GmO structure is mechanically stable.

Modeling of isolated β-GmO bilayers (with 25 Å of vacuum between them as in the case of monolayers) included

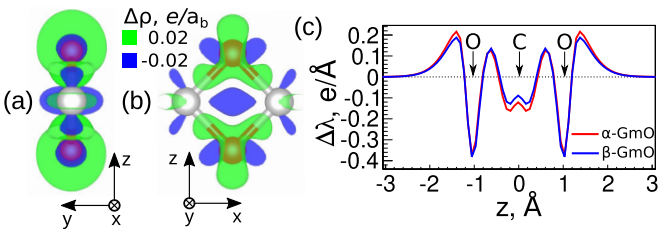

FIG. 4. (a) Front view and (b) side view of the change of electron density distribution, $\Delta\rho$, in β-GmO compared to free C and O atoms. (c) Change in the planar-averaged electron density, $\Delta\lambda(z)$, for the α- and β-phases of GmO. Arrows indicate the z-coordinates of the atoms.

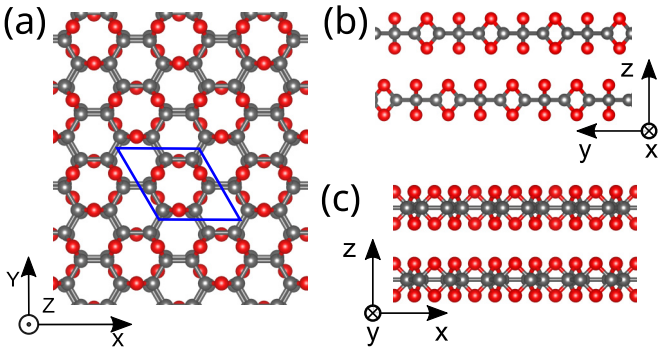

FIG. 5. β-GmO bilayer: (a) top view, (b) side view along the armchair direction, and (c) side view along the zigzag direction. The same AB arrangement of the layers is present in the AB-stacked β-GmO multilayer system. (Primitive cell borders: blue; C: gray; O: red.)

Grimme's DFT-D3 van der Waals correction [21] with Becke-Jonson (BJ) [22] damping. The results demonstrated that two layers of β-GmO prefer to align by translating with respect to each other in the way that brings lower O atoms of the upper monolayer above C – C bridges without O atoms of the lower monolayer [Fig. 5(a)]; i.e., this AB-stacking corresponds to a translation vector $\boldsymbol{T} = 2/3\boldsymbol{a_1} + 1/3\boldsymbol{a_2}$ of one of the monolayers with respect to another, where $\boldsymbol{a_1}$ and $\boldsymbol{a_2}$ are real space lattice vectors and $|\boldsymbol{a_1}| = |\boldsymbol{a_2}| = a_{\text{lat}}$. The relaxed bilayer interplanar distance was found to be 4.65 Å for this translation vector, and formation energy per atom was $\Delta E = -0.53$ eV, which is only 0.02 eV more negative than the β-GmO monolayer formation energy, indicating that the layers are weakly bound.

Tests of 3D solids with up to four monolayers per supercell showed that although the AB bilayer was the most binding, it can be seen from Table II that AB-stacking does not have a big energetic advantage compared to AA- and ABC-stacking. This weak interlayer binding confirms the 2D nature of β-GmO and suggests that it is unlikely that β-GmO has a highly ordered 3D solid form.

B. Experimentally measured & simulated SAED patterns

The 2D single crystal spot diffraction patterns [Fig. 6(a)], obtained from TEM and SAED measurements on electron-transparent GmO-containing nanocomposite samples could not be interpreted by the relaxed or constrained α-GmO structures [diffraction rings III and IV in Fig. 6(b) corresponding to 2.54 Å and 1.47 Å], nor by coexisting graphene regions [rings I and II in Fig. 6(b) corresponding to 2.13 Å and 1.23 Å] seen

TABLE II. Parameters for different multilayer stacking of β-GmO layers as 3D solids.

Stacking	Formation Energy eV/atom	Interlayer spacing Å
AA	−0.51	5.1
AB	−0.53	4.6
ABC	−0.52	4.6

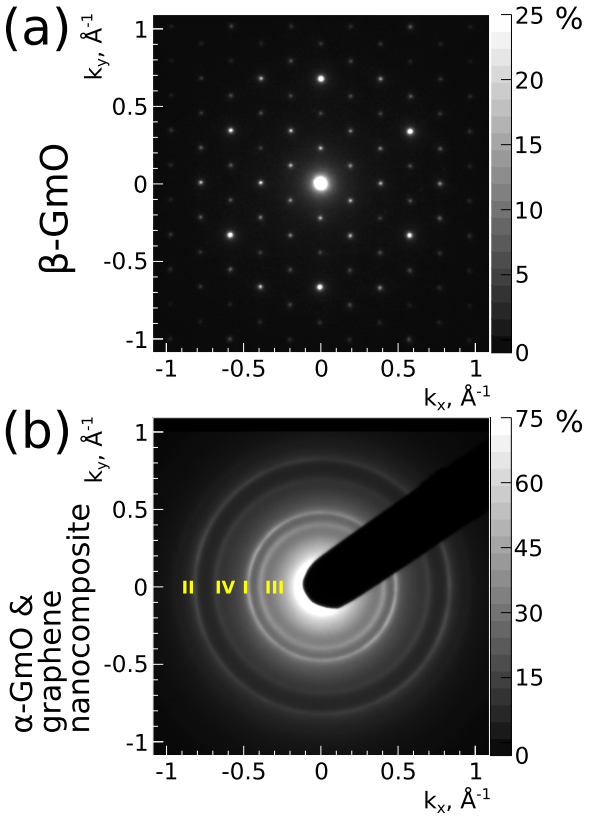

FIG. 6. Experimental SAED pattern of (a) a microparticle in Fig. 7 containing β-GmO layers and (b) α-GmO & graphene nanocomposite. First six diffraction spots from the innermost hexagon in (a) correspond to spacing 4.51 Å, the next two sets of diffraction spots correspond to 2.60 Åand 2.26 Å spacings. In (b), rings I and II correspond to 2.13 Å and 1.23 Å spacings of graphene, and rings III and IV correspond to 2.54 Å and 1.47 Å spacings of constrained α-GmO$^{120^\circ}$ that has that same unit cell area as fully relaxed α-GmO. Intensity scale bar is set with respect to the brightest intensity excluding the intensity of the central spot.

in the dominant 2D polycrystalline ring diffraction patterns [Fig. 6(b)]. The presence of continuous rings in the SAED data from Fig. 6(b) implied many randomly rotated α-GmO and graphene domains within the same imaged area. Simplified representation of the rotated α-GmO domains would be analogous to rotated graphene domains shown in Fig. 2(a). In contrast, the single-spot pattern in Fig. 6(a) provides evidence of an ordered single-phase structure.

The measured reciprocal lattice spacings and angles from more than 20 equivalent SAED spot patterns, when converted to real space (see Table III), did not match the α-GmO or graphene spacings, but had ratios close to a $(\sqrt{3} \times \sqrt{3})$ R30° relationship, as predicted by DFT for β-GmO. Figure 7 shows amplitude contrast bright field TEM (a) and phase contrast HRTEM (b) images of a typical β-GmO particle giving the typical electron diffraction pattern in Fig. 6(a). Direct lattice spacing measurements from HRTEM images fit the unit cell dimensions from *ab initio* computations [Fig. 7(b) and Table III]. The contrast in HRTEM is indicative of layers that are translated with respect to each other and give Moiré-like contrast. While all of the experimental data can be interpreted

TABLE III. Experimentally observed SAED (exp) and simulated theoretical (th) spacings of the sample containing β-GmO. Colors refer to the spacings from HRTEM Fig. 7(b).

k_{exp} 1/Å	d_{exp}, Å	k_{th}, 1/Å	d_{th}, Å	(h, k)[a]
0.22	4.51	0.22	4.46	$(\pm1, 0), (0, \pm1), (\pm1, \mp1)$
0.38	2.60	0.39	2.59	$(\pm2, \mp 1), (\pm1, \mp 2), (\pm1, \pm 1)$
0.44	2.26	0.45	2.24	$(\pm2, 0), (0, \pm2), (\pm2, \mp2)$
0.59	1.71	0.59	1.70	$(\pm3, \mp1), (\pm1, \mp3), (\pm3, \mp2),$ $(\pm2, \mp3), (\pm2, \pm1), (\pm1, \pm2)$
0.66	1.51	0.67	1.49	$(\pm3, 0), (0, \pm3), (\pm3, \mp3)$
0.77	1.31	0.77	1.30	$(\pm4, \mp2), (\pm2, \mp4), (\pm2, \pm2)$
0.80	1.26	0.80	1.24	$(\pm4, \mp1), (\pm1, \mp4), (\pm4, \mp3),$ $(\pm3, \mp4), (\pm3, \pm1), (\pm1, \pm3)$
0.88	1.13	0.89	1.12	$(\pm4, 0), (0, \pm4), (\pm4, \mp4)$
0.96	1.03	0.97	1.03	$(\pm5, \mp2), (\pm2, \mp5), (\pm5, \mp3),$ $(\pm3, \mp5), (\pm3, \pm2), (\pm2, \pm3)$

[a]Vectors $\boldsymbol{b}_1$ and $\boldsymbol{b}_2$ are reciprocal to the primitive vectors of the direct lattice shown in Fig. 1(c), and $|\boldsymbol{b}_1| = |\boldsymbol{b}_2|$. Indices h and k define reciprocal lattice vectors as $\boldsymbol{G} = h\boldsymbol{b}_1 + k\boldsymbol{b}_2$.

in a self-consistent way using the DFT-predicted unit cell of β-GmO, the most convincing proof is seen when the experimental SAED pattern [Fig. 6(a)] is compared to the one calculated for the β-GmO monolayer [Fig. 8(a)], confirming that all reciprocal space points match each other.

As the selected area aperture of 0.5 μm was shifted across the > 2 μm particle, the spot diffraction pattern kept the same geometry, indicating that β-GmO monolayers can be many microns in width. However, the relative intensities of the diffraction spots changed with tilting (not shown here), because different parts of a β-GmO particle had different projected thicknesses. Hence, different numbers of layers in the local multilayer stacked. The spot intensities also changed with tilting of any given sample area, but the spot positions and angles remained essentially unchanged over $\pm20^\circ$ of tilting in two perpendicular directions. Tilting experiments proved that the single crystal β-GmO structure was two-dimensional in real space, with a reciprocal lattice made of

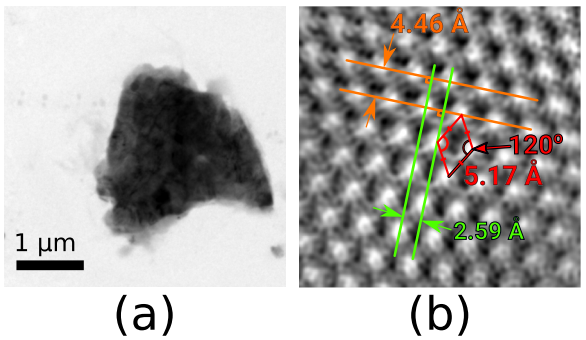

FIG. 7. Experimental TEM images of a particle composed of many stacked β-GmO monolayers in the electron beam direction: (a) bright field and (b) high-resolution electron microscopy photo. (Red: primitive cell and lattice parameters; orange and green: planes and spacings corresponding to the 1st and 2nd diffraction spots from Table III, respectively.)

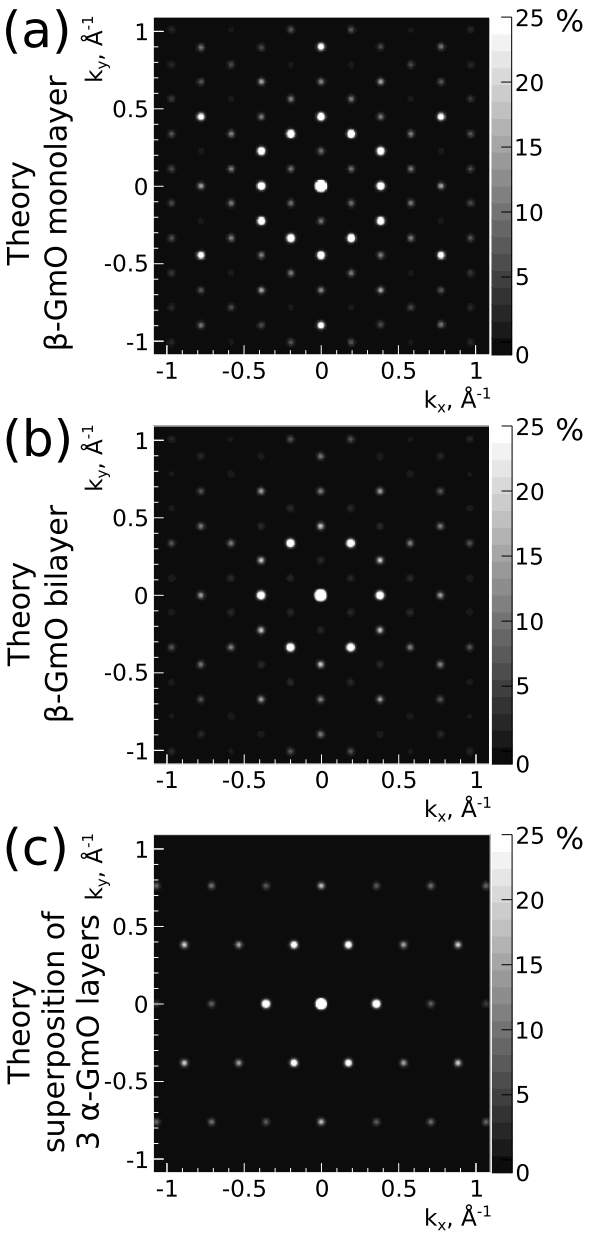

FIG. 8. Theoretically predicted SAED patterns of (a) β-GmO monolayer, (b) β-GmO bilayer from Fig. 5, and (c) superposition of three equivalent α-GmO monolayers differing by 60° rotation. First six visible β-GmO diffraction spots from the innermost hexagon in (a) and (b) correspond to spacing 4.46 Å, the next two sets of dominant diffraction spots correspond to 2.59 Å and 2.24 Å spacings. The first two dominant sets of diffraction spots for α-GmO in (c) correspond to spacings of 2.84 Å and 1.32 Å. For α-GmO$^{120^\circ}$, the first two spacings would be 2.55 Å and 1.47 Å. Intensity scale bar is set with respect to the brightest intensity excluding the intensity of the central spot.

rods that were continuously cut by the Ewald sphere as the sample was being tilted.

Table III provides spacings in reciprocal and direct space for the experimental diffraction pattern [Fig. 6(a)] and theoretically computed for the β-GmO monolayer [Fig. 8(a)], and also assigns (h, k) indices to all the spots. The experimental and theoretical peak positions are in excellent

agreement; visual variations in intensities between the experimental [Fig. 6(a)] and theoretical [Fig. 8(a)] patterns can be explained by the fact that SAED experimental measurements were taken from particles containing tens to hundreds of β-GmO monolayers with many different relative alignments. Although varying the number of layers does not change the positions of the allowed peaks, the relative positioning of additional layers influences the intensities of the diffraction pattern; for example, the simulated diffraction pattern for the β-GmO bilayer from Fig. 5 with the corresponding computed intensities is shown in Fig. 8(b), demonstrating that a bilayer is distinguishable from a monolayer by the diffraction intensities. In the present case, fortunately, additional layers did not cause any of the theoretical peaks to disappear through destructive interference. Notably, the presence of multiple layers, confirmed by HRTEM, did not alter the SAED spot positions and did not turn them into rings. The latter indicates that β-GmO layers prefer translations with respect to each other rather than rotations (different from the symmetry-equivalent ones).

Figure 8(c) shows the simulated diffraction pattern for the superposition of three α-GmO layers differing by 60° rotation around the axis perpendicular to the plane of layers. The most dominant diffraction spacings are 2.84 Å and 1.32 Å. The diffraction pattern for constrained α-GmO$^{120^\circ}$ layers look similar, with the most dominant spacings at 2.55 Å and 1.47 Å [like the experimental spacings in Fig. 6(b)]. The α-GmO diffraction patterns do not have peaks around 4.46 Å, 2.24 Å, and 1.70 Å that are pertinent to β-GmO structure.

Experimentally, the β-GmO particles in the investigated samples are stable: the same samples were remeasured with TEM after ∼2 years in storage at ambient temperature and pressure, and the same β-GmO HRTEM images and diffraction patterns with corresponding spacings and spot positions were found.

C. Band structure, density of states, and 2D Young's modulus

Our DFT calculations predict that pure β-GmO monolayer is a semiconductor with a 1.18 eV direct band gap at the Γ-point. Figure 9(a) shows the β-GmO band structure unfolded into the α-GmO primitive cell via the band unfolding technique [23–26]. During bright field TEM and HRTEM imaging of particles containing β-GmO, there was evident charging effects, providing experimental proof of the semiconducting/insulating nature of β-GmO.

In contrast, a fully relaxed α-GmO monolayer, with lattice constant $a_{\text{lat}} = 3.13$ Å and opening angle $\alpha = 130^\circ$, is a semiconductor with a 3.03 eV direct band gap at the Γ-point and an indirect band gap of 0.58 eV for the M_1–Γ transition [Fig. 9(b)] [1,3]. However, the α-GmO monolayer with the same area and constrained to have $a_{\text{lat}} = 2.95$ Å and $\alpha = 120^\circ$ is a conductor [Fig. 9(c)] since the band gap closes at the M_1 point.

The α- and β-GmO densities of states normalized to a 1,3-dioxetane unit is shown in Fig. 10. β-GmO has states just below the Fermi level closer to the Fermi level, as well as both bonding and anti-bonding O 2s peaks about 1.5 eV closer to the Fermi level in β-GmO. Table IV lists the O 2s peak positions computed from the density of states; α- and

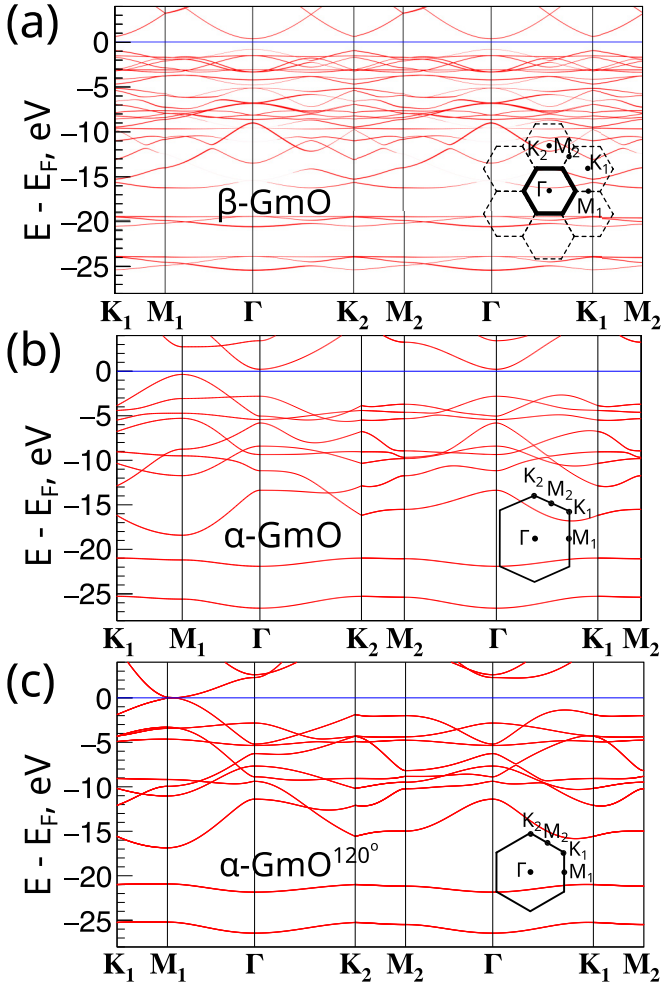

FIG. 9. Band structure of the (a) fully relaxed β-GmO monolayer with $a_{\text{lat}} = 5.17$ Å and $\alpha = 120^\circ$, (b) fully relaxed α-GmO monolayer with $a_{\text{lat}} = 3.13$ Å and $\alpha = 130^\circ$, and (c) constrained α-GmO monolayer with $a_{\text{lat}} = 2.95$ Å and $\alpha = 120^\circ$. Energies are given relative to the Fermi level. The areas of the unit cell of the fully relaxed and constrained α-GmO monolayers are the same.

β-GmO might be distinguished by the O 2s (and O 1s) peaks in x-ray photoelectron spectroscopy. However, the splitting between bonding and anti-bonding O 2s peaks of about 4.5 eV

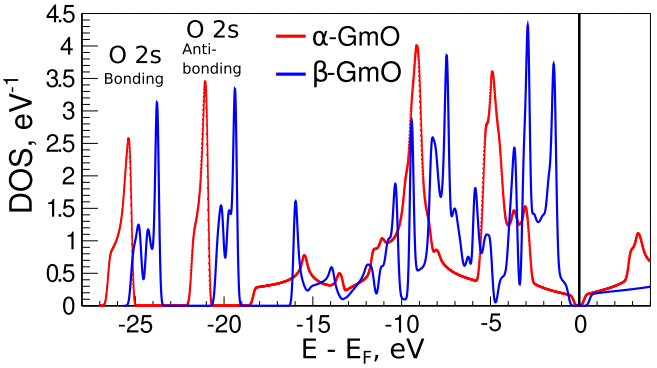

FIG. 10. Density of states (per α-GmO formula unit) for the fully relaxed α-GmO monolayer, β-GmO monolayer. Fermi energy is at 0 eV.

TABLE IV. Weighted centers and splittings of the O 2s bonding and anti-bonding peaks for α- and β-GmO. All energies in eV.

Structure	E_{O2s}^{Bonding}	$E_{O2s}^{\text{Anti-bonding}}$	$\Delta E_{O2s}^{\text{Split}}$
α-GmO	−25.70	−21.24	4.46
β-GmO	−24.24	−19.71	4.53

(arising in the common 1,3-dioxetane unit) is the same for both structures and cannot be used to distinguish the two.

The computed 2D Young's modulus of β-GmO monolayer in both the armchair and zigzag directions was found to be 212 N/m, while for α-GmO the Young's modulus was computed to be 283 N/m in the armchair and 210 N/m in zigzag directions. Compared to a value of around 350 N/m for graphene [27], β-GmO is much softer.

IV. CONCLUSIONS

This work reports the experimental discovery of a high-symmetry D_{6h} form of two-dimensional solid CO, named β-GmO, from selected area high energy transmission electron diffraction and high resolution transmission electron microscopy, and the determination of its basic properties via DFT calculations. The material was produced by COnovate Inc. and kept at atmospheric conditions until TEM measurements were performed at ambient temperature and about 10^{-5} Pa pressure. After the initial experiments, the samples, stored at ambient temperature and pressure and remeasured after ∼2 years, gave identical experimental results, indicating that the material is stable.

Taken together with the prior discovery of the D_{2h} form, α-GmO, the new β-GmO monolayer form demonstrates that solid CO can have more than one 2D GmO crystal phase, similar to the situation for 3D-CO. These two 2D-GmO crystal phases, generated from the same basic structural building block, can be considered as molecular crystals, like the majority of the 3D-CO crystal phases.

Experimentally measured SAED spot positions and angles coincided with those computed for the structure predicted by DFT for a hexagonal unit cell with lattice constant of 5.17 Å. HRTEM imaging confirmed the lattice constant of β-GmO. That the positions of the SAED spots did not change during sample tilting in TEM proved that β-GmO is composed of solid CO in the form of 2D monolayers that are translated with respect to each other, unlike the case of α-GmO where 2D domains are rotated within and between layers resulting in SAED ring patterns. *Ab initio* multilayer simulations showed that the interlayer binding energies of the β-GmO layers are weak, and thus β-GmO is unlikely to form ordered three-dimensional solid crystal structures.

From the calculated band structure, β-GmO monolayer is predicted to be semiconducting, with a direct band gap of ∼1.2 eV that is larger than the indirect band gap of 0.6 eV of α-GmO. β-GmO bonding and anti-bonding density of states O 2s peaks demonstrate about 1.5 eV shift with respect to the ones in α-GmO. The latter shift could be detected in x-ray photoelectron spectroscopy.

Due to lower 2D Young's modulus in armchair direction, β-GmO monolayer is generally softer than both graphene and α-GmO.

ACKNOWLEDGMENTS

This work was supported by the National Science Foundation (Grants No. EFMA-1741673 and No. IIP-1843306).

[1] E. C. Mattson, H. Pu, S. Cui, M. A. Schofield, S. Rhim, G. Lu, M. J. Nasse, R. S. Ruoff, M. Weinert, M. Gajdardziska-Josifovska, J. Chen, and C. J. Hirschmugl, Evidence of nanocrystalline semiconducting graphene monoxide during thermal reduction of graphene oxide in vacuum, ACS Nano **5**, 9710 (2011).

[2] H. H. Pu, E. C. Mattson, S. H. Rhim, M. Gajdardziksa-Josifovska, C. J. Hirschmugl, M. Weinert, and J. H. Chen, First-principles studies on infrared properties of semiconducting graphene monoxide, J. Appl. Phys. **114**, 164313 (2013).

[3] H. H. Pu, S. H. Rhim, C. J. Hirschmugl, M. Gajdardziska-Josifovska, M. Weinert, and J. H. Chen, Strain-induced band-gap engineering of graphene monoxide and its effect on graphene, Phys. Rev. B **87**, 085417 (2013).

[4] H. H. Pu, S. H. Rhim, C. J. Hirschmugl, M. Gajdardziska-Josifovska, M. Weinert, and J. H. Chen, Anisotropic thermal conductivity of semiconducting graphene monoxide, Appl. Phys. Lett. **102**, 223101 (2013).

[5] C. S. Jamieson, A. M. Mebel, and R. I. Kaiser, Understanding the kinetics and dynamics of radiation-induced reaction pathways in carbon monoxide ice at 10 K, The Astrophysical Journal Supplement Series **163**, 184 (2006)

[6] J. B. Dalton, Spectroscopy of icy moon surface materials, Space Sci. Rev. **153**, 219 (2010).

[7] D. T. Cromer, D. Schiferl, R. LeSar, and R. L. Mills, Room-temperature structure of carbon monoxide at 2.7 and 3.6 GPa, Acta Crystallographica Section C **39**, 1146 (1983).

[8] Mills, R. L., Schiferl, D., Katz, A. I., and Olinger, B. W., New phases and chemical reactions in solid CO under pressure, J. Phys. Colloques **45**, C8 (1984).

[9] A. I. Katz, D. Schiferl, and R. L. Mills, New phases and chemical reactions in solid carbon monoxide under pressure, J. Phys. Chem. **88**, 3176 (1984).

[10] J. Sun, D. D. Klug, C. J. Pickard, and R. J. Needs, Controlling the Bonding and Band Gaps of Solid Carbon Monoxide with Pressure, Phys. Rev. Lett. **106**, 145502 (2011).

[11] G. Frapper, C.-X. Cu, M. Kertesz, J.-F. Halet, J.-Y. Saillard, G. Frapper, and C.-X. Cu, Can carbon monoxide polymerize? A theoretical investigation of polyketone, Chem. Commun. **20**, 2011 (1997).

[12] K. Xia, J. Sun, C. J. Pickard, D. D. Klug, and R. J. Needs, Ground state structure of high-energy-density polymeric carbon monoxide, Phys. Rev. B **95**, 144102 (2017).

[13] H. J. Xiang, S.-H. Wei, and X. G. Gong, Structural motifs in oxidized graphene: A genetic algorithm study based on density functional theory, Phys. Rev. B **82**, 035416 (2010).

[14] P. Giannozzi, S. Baroni, N. Bonini, M. Calandra, R. Car, C. Cavazzoni, D. Ceresoli, G. L. Chiarotti, M. Cococcioni,

I. Dabo, A. D. Corso, S. de Gironcoli, S. Fabris, G. Fratesi, R. Gebauer, U. Gerstmann, C. Gougoussis, A. Kokalj, M. Lazzeri, L. Martin-Samos *et al.*, QUANTUM ESPRESSO: a modular and open-source software project for quantum simulations of materials, J. Phys.: Condens. Matter **21**, 395502 (2009).

[15] P Giannozzi Jr, O. Andreussi, T. Brumme, O. Bunau, M. B. Nardelli, M. Calandra, R. Car, C. Cavazzoni, D. Ceresoli, M. Cococcioni, N. Colonna, I. Carnimeo, A. D. Corso, S. de Gironcoli, P. Delugas, R. A. DiStasio, A. Ferretti, A. Floris, G. Fratesi, G. Fugallo *et al.*, Advanced capabilities for materials modelling with QUANTUM ESPRESSO, J. Phys.: Condens. Matter **29**, 465901 (2017).

[16] A. Kokalj, XCrySDen – a new program for displaying crystalline structures and electron densities, J. Mol. Graphics Modell. **17**, 176 (1999).

[17] K. Momma and F. Izumi, *VESTA3* for three-dimensional visualization of crystal, volumetric and morphology data, J. Appl. Crystallogr. **44**, 1272 (2011).

[18] A. D. Corso, Pseudopotentials periodic table: From H to Pu, Comput. Mater. Sci. **95**, 337 (2014).

[19] L.-M. Peng, G. Ren, S. L. Dudarev, and M. J. Whelan, Robust parameterization of elastic and absorptive electron atomic scattering factors, Acta Crystallogr D Biol Crystallogr **52**, 257 (1996).

[20] C. J. Hirschmugl, M. Gajdardziska-Josifovska, M. Schofield, Y. Kutsovsky, X. Huang, and D. Radevych, Graphene monoxide compositions of matter and electrodes comprising them, U.S. patEnt Application Number 17/148010, COnovate, Inc., University of Wisconsin-Milwaukee Research Foundation, 2021.

[21] S. Grimme, J. Antony, S. Ehrlich, and H. Krieg, A consistent and accurate ab initio parametrization of density functional dispersion correction (DFT-D) for the 94 elements H-Pu, J. Chem. Phys. **132**, 154104 (2010).

[22] S. Grimme, S. Ehrlich, and L. Goerigk, Effect of the damping function in dispersion corrected density functional theory, J. Comput. Chem. **32**, 1456 (2011).

[23] J. W. Davenport, R. E. Watson, and M. Weinert, Linear augmented-Slater-type-orbital method for electronic-structure calculations. V. Spin-orbit splitting in Cu_3 Au, Phys. Rev. B **37**, 9985 (1988).

[24] Y. Qi, S. H. Rhim, G. F. Sun, M. Weinert, and L. Li, Epitaxial Graphene on SiC(0001): More than Just Honeycombs, Phys. Rev. Lett. **105**, 085502 (2010).

[25] M. Chen and M. Weinert, Layer k-projection and unfolding electronic bands at interfaces, Phys. Rev. B **98**, 245421 (2018).

[26] M. X. Chen and M. Weinert, Revealing the substrate origin of the linear dispersion of silicene/Ag(111), Nano Lett. **14**, 5189 (2014).

[27] C. Lee, X. Wei, J. W. Kysar, and J. Hone, Measurement of the elastic properties and intrinsic strength of monolayer graphene, Science **321**, 385 (2008).